The *Escherichia coli* RnlA–RnlB toxin–antitoxin complex: production, characterization and crystallization

Gabriela Garcia-Rodriguez,[a,b] Ariel Talavera Perez,[a,b] Albert Konijnenberg,[a,b,c] Frank Sobott,[c,d,e] Jan Michiels[f,g] and Remy Loris[a,b]*

[a]Structural Biology Brussels, Vrije Universiteit Brussel, Pleinlaan 2, B-1050 Brussels, Belgium, [b]Center for Structural Biology, VIB, Pleinlaan 2, B-1050 Brussels, Belgium, [c]Department of Chemistry, University of Antwerp, Antwerp, Belgium, [d]The Astbury Centre for Structural Molecular Biology, University of Leeds, Leeds, England, [e]School of Molecular and Cellular Biology, University of Leeds, Leeds, England, [f]Center for Microbiology, VIB, B-3000 Leuven, Belgium, and [g]Center for Microbial and Plant Genetics, KU Leuven, B-3000 Leuven, Belgium. *Correspondence e-mail: remy.loris@vub.be

The *Escherichia coli rnlAB* operon encodes a toxin–antitoxin module that is involved in protection against infection by bacteriophage T4. The full-length RnlA–RnlB toxin–antitoxin complex as well as the toxin RnlA were purified to homogeneity and crystallized. When the affinity tag is placed on RnlA, RnlB is largely lost during purification and the resulting crystals exclusively comprise RnlA. A homogeneous preparation of RnlA–RnlB containing stoichiometric amounts of both proteins could only be obtained using a His tag placed C-terminal to RnlB. Native mass spectrometry and SAXS indicate a 1:1 stoichiometry for this RnlA–RnlB complex. Crystals of the RnlA–RnlB complex belonged to space group $C2$, with unit-cell parameters $a = 243.32$, $b = 133.58$, $c = 55.64$ Å, $\beta = 95.11°$, and diffracted to 2.6 Å resolution. The presence of both proteins in the crystals was confirmed and the asymmetric unit is likely to contain a heterotetramer with $RnlA_2$:$RnlB_2$ stoichiometry.

1. Introduction

Bacterial toxin–antitoxin (TA) modules are small operons encoding a toxin that interferes with vital cell processes and an antitoxin that counteracts this toxic activity (for reviews, see Harms *et al.*, 2018; Unterholzner *et al.*, 2013; Van Melderen, 2010; Yamaguchi & Inouye, 2011). Currently, six classes of TA systems have been identified based on the nature of the antitoxin (protein or RNA) and the mechanisms that they use to neutralize the activities of their cognate toxins (for reviews, see Otsuka, 2016; Page & Peti, 2016). Type II TA systems form the largest and most studied class of TA systems, with both the toxin and the antitoxin being proteins. While originally limited to a small number of families, currently at least 20 distinct type II TA families can be distinguished based on the phylogeny and activity of their toxin (Guglielmini & Van Melderen, 2011). The antitoxins in this class directly bind and inhibit the toxin (for reviews, see Loris & Garcia-Pino, 2014; Page & Peti, 2016).

Next to the null hypothesis that they are selfish genetic elements, three major classes of biological functions have so far been proposed for TA modules (Van Melderen & Saavedra De Bast, 2009). The first is the stabilization of mobile genetic elements and unstable sections of chromosomes. They were initially discovered on plasmids, which they stabilize via a mechanism of post-segregational killing (Gerdes *et al.*, 1986).

research communications
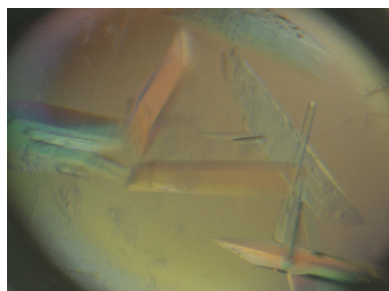
A second possibility that has been proposed many times is that they function in stress response and in the formation of persisters (for a review, see Gerdes *et al.*, 2005). Mutants of the *Escherichia coli hipAB* TA module are known to have a persister phenotype (Moyed & Bertrand, 1983; Korch *et al.*, 2003), but the link between other TA modules and persistence in *E. coli* is weak (Ramisetty *et al.*, 2016; Goormaghtigh *et al.*, 2018). Yet certain TA modules in *Salmonella* have been shown to contribute to the formation of persisters in macrophages (Helaine *et al.*, 2014), and the *mqsRA* module also regulates persister formation in *Pseudomonas putida* (Sun *et al.*, 2017).

The third major function that has been proposed for TA modules is protection against bacteriophages. A role in bacterial suicide upon phage infection was first suggested for *E. coli mazEF* (Hazan & Engelberg-Kulka, 2004). Since then, TA-mediated abortive phage infection has been observed for class II, III and IV TA modules (for a review, see Dy *et al.*, 2014). This observation is important with regard to the renewed interest in phage therapy following increasing multidrug resistance in bacterial pathogens. Abortive phage infection presents a potential obstacle to treating recalcitrant infections using this approach (Dy *et al.*, 2014).

The *E. coli rnlAB* operon, together with *lsoAB* from the cryptic *E. coli* plasmid pOSAK1, represents a poorly studied family of type II TA systems in which *rnlA* encodes an endoribonuclease (initially called RNase LS) and *rnlB* translates into its cognate antitoxin RnlB, which can directly bind and neutralize RnlA (Otsuka & Yonesaki, 2005; Otsuka *et al.*, 2007; Koga *et al.*, 2011). Unlike most TA modules, the *rnlAB* operon is not autoregulated. Rather, evidence has been provided that IscR, an Fe–S cluster protein, acts as a repressor of the *rnlAB* operon (Otsuka *et al.*, 2010). IscR is a transcription factor that controls the expression of genes that are necessary for Fe–S cluster biogenesis, and the biological link to *rnlAB* remains unclear. σ^{32}, which controls heat-shock response, has also been suggested to control *rnlA* expression, but loose ends also remain here (Nonaka *et al.*, 2006).

Like the related *lsoAB*, the *rnlAB* module acts as an abortive infection system in *E. coli* against a T4 *dmd* mutant phage (Otsuka & Yonesaki, 2012). Following infection by a T4 *dmd* mutant, RnlB is rapidly degraded, causing the activation of RnlA. The endoribonucleotidic activity of RnlA leads to the rapid degradation of late T4 mRNAs, which results in the arrest of T4 phage propagation. However, wild-type T4 phage can normally infect *E. coli* cells thanks to its own phage antitoxin, Dmd, that binds and inhibits RnlA as well as its homologue LsoA. This promiscuous phage antitoxin constitutes a powerful counterpart to the toxin defences of the host, successfully guaranteeing the propagation of the infection. Hence, it is not surprising that almost all enterobacteria phages contain Dmd homologues. Wei *et al.* (2016) reported a sequence alignment including Dmd sequences from 22 *Enterobacteria* phages, three *Yersinia* phages and two *Shigella* phages, which illustrates the distribution of this gene across phage classes and strongly suggests the involvement of RnlA as well as LsoA in defence mechanisms against various bacteriophage infections.

In order to understand RnlA-mediated protection against T4 phages at the molecular level, structures of the individual proteins (RnlA, RnlB and Dmd) and their complexes are required. Currently, structures of the isolated RnlA protein and of isolated Dmd are available (Wei *et al.*, 2013, 2016), as well as that of an LsoA–Dmd complex (Wan *et al.*, 2016). Previous attempts to obtain a structure of the RnlA–RnlB complex failed because RnlB is apparently highly unstable and degrades prior to and/or during purification, leading to a preparation that essentially contains only RnlA (Wei *et al.*, 2016). Here, we present the production, characterization and crystallization of a stable stoichiometric RnlA–RnlB toxin–antitoxin complex.

2. Materials and methods

2.1. Cloning, protein expression and purification

The coding region for the *rnlA-rnlB* operon (UniProtKB accession Nos. NP_417119.1 and NP_417120.2, respectively) was amplified from the *E. coli* K12 chromosome and introduced into a pET-28a vector using NdeI and HindIII restriction sites and the primers 5′-CACCCATATGACAATCAGG AGTTACAAAAA-3′ (forward) and 5′-GATCAAGCTTTCA AAAATCCATTGACAGGA-3′ (reverse). This cloning places a His tag followed by a thrombin-cleavage site (MGSSHHH HHHSSGLVPRGSH) at the N-terminus of RnlA. This construct is referred to as His-RnlA–RnlB in Table 1. The corresponding proteins will be referred to as His-RnlA and RnlB.

The *rnlA-rnlB* bicistronic gene was again amplified from the previous expression plasmid pET-28a-*rnlA-rnlB* using the primers 5′-GACTAGCATATGACAATCAGGAGTTACAA AAACTTA-3′ (forward) and 5′-GACGAAGCGGCCGCAA AATCCATTGACAGGACTTGG-3′ (reverse), which insert restriction sites for NdeI and NotI, and cloned into a pET-21b vector. This construct (referred to as RnlA–RnlB-His in Table 1) places a noncleavable 6×His tag at the C-terminus of RnlB (AAALEHHHHHH). The corresponding proteins will be referred to as RnlA and RnlB-His. All constructs were checked by DNA sequencing using specific vector primers after transformation into the expression strains.

The expression plasmids were transformed into *E. coli* BL21 (DE3) competent cells (Studier *et al.*, 1990) using the CaCl$_2$ method (Hanahan *et al.*, 1991). Transformed colonies were selected on LB plates containing ampicillin (100 µg ml^{-1}) or kanamycin (50 µg ml^{-1}), according to the vector, and 2%(*w*/*v*) glucose and grown overnight at 310 K. A 120 ml preculture was started from one isolated colony inoculated into LB medium supplemented with 100 µg ml^{-1} ampicillin or 50 µg ml^{-1} kanamycin and 0.2%(*w*/*v*) glucose and grown overnight at 310 K with aeration. A 100-fold dilution of the preculture was used to start 12 bottles of 1 l LB culture containing 100 µg ml^{-1} ampicillin or 50 µg ml^{-1} kanamycin and 0.2%(*w*/*v*) glucose. The cells were grown at 310 K with aeration until the OD$_{600}$ reached 0.6. The temperature was then decreased to 289 K and the cultures

Table 1
Macromolecule-production information.

Construct	His-RnlA–RnlB	RnlA–RnlB-His
Source organism	*E. coli* (strain K12)	*E. coli* (strain K12)
DNA source	K12 chromosome	K12 chromosome
Forward primer	5′-CACC**CATATG**ACAATCAGGAGTTACAAAAA-3′	5′-GACTAG**CATATG**ACAATCAGGAGTTACAAAAACTTA-3′
Reverse primer	5′-GATC**AAGCTT**TCAAAAATCCATTGACAGGA-3′	5′-GACGAA**GCGGCCGC**AAAATCCATTGACAGGACTTGG-3′
Cloning vectors	pET-28a	pET-21b
Expression vectors	pET-28a	pET-21b
Expression host	*E. coli* BL21 (DE3)	*E. coli* BL21 (DE3)
Complete amino-acid sequences of the expressed proteins		
His-thrombin-RnlA	MGSSHHHHHHSSGLVPRGSHMTIRSYKNLNLVRANIETESRQFIEN KNYSIQSIGMPGSRAGLRVVFTRPGVNLATVDIFYNGDGSTTI QYLTGANRSLGQELADHLFETINPAEFEQVNMVLQGFVETSVLP VLELSADESHIEFREHSRNAHTVVWKIISTSYQDELTVSLHITT GKLQIQGRPLSCYRVFTFNLAALLDLQGLEKVLIRQEDGKANIV QQEVARTYLQTVMADAYPHLHVTAEKLLVSGLCVKLAAPDLPDY CMLLYPELRTIEGVLKSKMSGLGMPVQQPAGFGTYFDKPAAHYI LKPQFAATLRPEQINIISTAYTFFNVERHSLFHMETVVDASRMI SDMARLMGKATRAWGIIKDLYIV	
RnlB	LFEITGINVSGALKAVVMATGFENPLSSVNEIETKLSALLGSETTG EILFDLLCANGPEWNRFVTLEMKYGRIMLDTAKIIDEQDVPTHI LSKLTFTLRNHPEYLEASVLSPDDVRQVLSMDF	
RnlA		MTIRSYKNLNLVRANIETESRQFIENKNYSIQSIGMPGSRAGLRV VFTRPGVNLATVDIFYNGDGSTTIQYLTGANRSLGQELADHLFE TINPAEFEQVNMVLQGFVETSVLPVLELSADESHIEFREHSRNA HTVVWKIISTSYQDELTVSLHITTGKLQIQGRPLSCYRVFTFNL AALLDLQGLEKVLIRQEDGKANIVQQEVARTYLQTVMADAYPHL HVTAEKLLVSGLCVKLAAPDLPDYCMLLYPELRTIEGVLKSKMS GLGMPVQQPAGFGTYFDKPAAHYILKPQFAATLRPEQINIISTA YTFFNVERHSLFHMETVVDASRMISDMARLMGKATRAWGIIKDL YIV
RnlB-His		LFEITGINVSGALKAVVMATGFENPLSSVNEIETKLSALLGSETTG EILFDLLCANGPEWNRFVTLEMKYGRIMLDTAKIIDEQDVPTHI LSKLTFTLRNHPEYLEASVLSPDDVRQVLSMDFAAALEHHHHHH

were left for a further 30 min before expression of the proteins was induced by adding 0.5 mM isopropyl β-D-1-thiogalacto-pyranoside (IPTG). The cells were harvested by centrifugation for 20 min at 6500g (5000 rev min^{-1} in a JLA-8.1000 rotor) and 277 K after overnight incubation at 289 K with aeration and were subsequently resuspended in lysis buffer (20 mM Tris–HCl pH 8, 500 mM NaCl, 2 mM β-mercapto-ethanol) and a protease-inhibitor cocktail (cOmplete, Sigma–Aldrich/Merck). The cells were lysed using a continuous-flow cell disruptor (Constant Systems) at 277 K and cell debris was removed by centrifugation for 45 min at 41 700g (18 000 rev min^{-1} in a JA-20 rotor) and 277 K. The cleared extract was loaded onto a nickel–nitrilotriacetic acid affinity column (connected to an ÄKTAexplorer FPLC system, GE Healthcare) pre-equilibrated in lysis buffer and washed with the same buffer to remove nonbinding contaminants. Proteins (which were assumed to be His-RnlA–RnlB or RnlA–RnlB-His complexes) were eluted using a linear imidazole gradient (0–500 mM) in 20 mM Tris–HCl pH 8, 500 mM NaCl, 2 mM β-mercaptoethanol) over 20 column volumes. The progress of the purification was analysed by SDS–PAGE (Laemmli, 1970) and a Western blot (Towbin *et al.*, 1979) with a mouse antibody recognizing the His tag (Bio-Rad, AbD Serotec). The fractions containing His-tagged protein were pooled and concentrated (Amicon UltraCel 10K) for subsequent size-exclusion chromatography (SEC). A Superdex 200 (16/60) column (GE Healthcare) was pre-equilibrated with SEC buffer [20 mM Tris–HCl pH 8, 150 mM NaCl, 1 mM tris(2-carboxyethyl)phosphine] and run at 1.0 ml min^{-1}. In the case of the RnlA–RnlB-His complex, the Superdex 200 fractions were pooled, concentrated and subsequently applied onto a Superdex 75 (16/60) column pre-equilibrated with SEC buffer. The fractions containing the presumed His-RnlA–RnlB and RnlA–RnlB-His complexes were pooled, flash-frozen and stored at 193 K.

2.2. Crystallization, X-ray data collection and processing

The protein samples in 20 mM Tris–HCl pH 8, 150 mM NaCl, 1 mM tris(2-carboxyethyl)phosphine were concentrated to 6–18 mg ml^{-1} for His-RnlA–RnlB and to 22–44 mg ml^{-1} for RnlA–RnlB-His. Crystallization conditions were initially screened using a Mosquito HTS robot from TTP Labtech (http://ttplabtech.com/) using 0.1 μl protein solution and 0.1 μl reservoir solution in a sitting drop equilibrated against 100 μl reservoir solution. Several commercially available screens were used: Crystal Screen, Crystal Screen 2, PEGRx HT and Index HT (Hampton Research), ProPlex, JCSG-*plus* and MIDAS (Molecular Dimensions) and JBScreen Classics 1–4 (Jena Biosciences). Silver Bullets (Hampton Research) was used as an additive screen during optimizations. Optimizations of promising hits were performed manually using the hanging-drop vapour-diffusion method in 48-well plates (Hampton VDX greased) with drops consisting of 0.5 μl protein solution and 0.5 μl reservoir solution equilibrated against 100 μl reservoir solution.

For data collection, crystals were flash-cooled in liquid nitrogen after being transferred to precipitant solution containing an additional cryoprotectant solution (20% PEG 400 for both His-RnlA–RnlB and RnlA–RnlB-His). Data for His-RnlA–RnlB were collected on beamline ID23-1 at the ESRF synchrotron facility, Grenoble, France, while data for RnlA–RnlB-His were measured on beamline PROXIMA-2A at the SOLEIL synchrotron facility, Gif-sur-Yvette, France. All data were indexed, integrated and scaled with *XDS* (Kabsch, 2010) via the *XDSME* interface (Legrand, 2017). Data quality and twinning were analyzed with *phenix.xtriage* (Liebschner *et al.*, 2019) and *POINTLESS* (Evans, 2006). Analysis of solvent contents was performed using the *CCP*4 program *MATTHEWS_COEF* (Kantardjieff & Rupp, 2003).

2.3. Mass-spectrometric analysis

2.3.1. Identification of RnlA and RnlB by LC-MS/MS mass spectrometry.
The protein solution was digested with trypsin and analysed by liquid-chromatographic tandem mass spectrometry on an LTQ XL IT mass spectrometer (Thermo Scientific, San José, California, USA) equipped with a microflow ESI source. Peptides were separated by an acetonitrile gradient on a C18 column and the MS scan routine was set to analyse the five most intense ions of each full MS scan by MS/MS. Dynamic exclusion was enabled to assure the detection of co-eluting peptides. Peak lists were generated using *extract-msn* (Thermo Scientific) within *Proteome Discoverer* 1.4.1. From the raw data files, MS/MS spectra were exported with the following settings: peptide mass range 350–5000 Da, minimal total ion intensity 500. The resulting peak lists were searched using *SequestHT* against a target-decoy RnlA6His protein database (RnlA entries comprising forward and reversed sequences). The following parameters were used: trypsin was selected with proteolytic cleavage only after arginine and lysine, the number of internal cleavage sites was set to 1, the mass tolerance for precursors and fragment ions was 1.0 Da, considered dynamic modifications of +15.99 Da for oxidized methionine. Peptide matches were filtered using the q-value and posterior error probability calculated by the *Percolator* algorithm ensuring an estimated false-positive rate of below 5%. The filtered *SequestHT* output files for each peptide were grouped according to the protein from which they were derived, and their individual number of peptide spectral matches was taken as an indicator of protein abundance.

2.3.2. Native mass-spectrometric analysis.
Native mass spectrometry was performed on a Synapt G2 mass spectrometer (Waters, Wilmslow, England). Samples were introduced into the gas phase at a concentration of 1.8 µM in 150 mM ammonium acetate pH 7.8 using nano-electrospray ionization with in-house-prepared gold-coated borosilicate glass capillaries. Crystals were pre-washed three times in water before being dissolved in 150 mM ammonium acetate pH 7.8. For the RnlA–RnlB-His sample before crystallization, the critical voltages throughout the instrument were a sampling-cone voltage of 25 V and a trap-collision energy of 10 V, whereas for

the sample with the redissolved RnlA–RnlB-His crystals these values were 120 V for the sampling-cone voltage and 5 V for the trap-collision energy, with pressures throughout the instrument of 5.7 and 0.0225 mbar for the source and trap-collision cell regions, respectively, in the case of the RnlA–RnlB-His sample before crystallization and 7 mbar and 0.0334 mbar for the source and trap-collision cell regions, respectively, in the case of the redissolved RnlA–RnlB-His crystals. Spectra were externally calibrated using a 10 mg ml^{-1} solution of caesium iodide. Analyses of the acquired spectra were performed using *MassLynx* v.4.1 (Waters). Native MS spectra were smoothed (to an extent depending on the size of the complexes) and additionally centred to calculate molecular weights.

2.4. Analytical size-exclusion chromatography and SDS–PAGE analysis of crystals

Analytical size-exclusion chromatography of His-RnlA–RnlB and RnlA–RnlB-His was performed on a Superdex Increase 200 column equilibrated with 20 mM Tris–HCl pH 8, 150 mM NaCl, 1 mM tris(2-carboxyethyl)phosphine. 0.5 ml sample injections were used at a flow rate of 0.75 ml min^{-1}. Bio-Rad gel-filtration standards (catalogue No. 1511901) were used to calibrate the column in the same buffer. Molecular weights were estimated according to Whitaker (1963).

SDS–PAGE analysis of crystals was performed in 15% gels. The crystals were prewashed three times in reservoir solution before being dissolved in water and subsequently run on a gel. Proteins were stained using Coomassie Blue.

2.5. Small-angle X-ray scattering (SAXS)

SAXS data for the His-RnlA–RnlB (2.5 mg ml^{-1}) and RnlA–RnlB-His (5.9 mg ml^{-1}) complexes were collected on beamline BM29 at the ESRF using the SEC–SAXS setup. Samples were applied onto a Shodex 4KW column that was run at 0.2 ml min^{-1} in 20 mM Tris–HCl pH 8, 150 mM NaCl, 1 mM tris(2-carboxyethyl)phosphine, 5% glycerol as the running buffer and the resulting peaks were directly measured in the X-ray beam. The final scattering curve was obtained by averaging the scattering curves covering a concentration range around the peak. Guinier plots were used to estimate R_g values and the I_0 values were estimated from extrapolation of the Guinier region to $q = 0$ as implemented in the *ATSAS* suite (Franke *et al.*, 2017).

3. Results and discussion

3.1. Purification and biophysical characterization of the His-RnlA–RnlB preparation

In our initial attempts to prepare and crystallize the RnlA–RnlB complex, we made a construct similar to that reported previously by Wei *et al.* (2013). A pET-28a plasmid containing the *rnlAB* operon cloned under the control of the T7 promoter, placing a His tag at the N-terminus of RnlA, was transformed into *E. coli* BL21 (DE3) cells for protein expression. The protein was purified by Ni–NTA affinity

chromatography followed by gel filtration. A total of 14 mg protein was obtained per litre of culture. The corresponding His-RnlA–RnlB preparation eluted from a Superdex Increase 200 column at a volume of 14.1 ml, which corresponds to an estimated molecular weight of 66 kDa (Fig. 1a). Considering that our construct renders His-RnlA with a monomeric mass of 42.3 kDa and RnlB with a mass of 13.7 kDa, this peak could correspond to a 1:1 stoichiometry of His-RnlA:RnlB. However, Coomassie Blue-stained SDS–PAGE gels of these fractions only showed a band corresponding to His-RnlA (Fig. 1b), as also confirmed by an anti-His-tag Western blot analysis.

The tryptic digest of the presumed His-RnlA–RnlB complex was analysed by LC tandem mass spectrometry in order to identify the components of the sample. A search of the resulting peak list against the recombinant His-RnlA sequence showed 87% coverage, including both the N-terminus and the C-terminus of the protein, indicating that no degradation was taking place. However, a search of the peak list against a target-decoy E. coli protein database showed the presence of only six unique RnlB peptides, which relates to the low search score observed for RnlB arising from its low relative abundance in the sample and possible degradation. It is worth mentioning that BL21 (DE3), the E. coli strain used for the expression of this construct, does not contain the rnlAB operon. Therefore, a low number of identified peptides correspond to recombinant RnlB protein.

SAXS data for the His-RnlA–RnlB sample (2.47 mg ml^{-1}) were collected on beamline BM29 at the ESRF. The scattering curve for this sample is rather noisy for q values larger than 0.16 Å^{-1} (Fig. 2a), but the Guinier plot shows a linear behaviour, rendering a radius of gyration (R_g) of 34.8 Å (Fig. 2b). The theoretical R_g for the crystallographic dimer in the published His-RnlA structure (PDB entry 4i8o; Wei et al., 2013) is 29.5 Å, while the theoretical R_g for the PDBePISA (https://www.ebi.ac.uk/pdbe/pisa/) biological assembly of PDB entry 4i8o shows a value of 34.6 Å, which is practically the same as our Guinier R_g for His-RnlA–RnlB. This observation strongly suggests the presence of the biological assembly of the RnlA dimer in solution and the absence of RnlB. Additionally, the molecular weight estimated from extrapolation to I_0 is 75 kDa, which points to the presence of a His-RnlA dimer rather than an equimolar complex between His-RnlA and RnlB. The χ^2 values for the fitting of the experimental scattering curve to the theoretical SAXS curves obtained from the published structure of the His-RnlA dimer (PDB entry 4i8o; Wei et al., 2013), for the crystallographic dimer as deposited and for the biological assembly involving dimerization via the C-terminal domain as generated via crystal symmetry, are 3.3 and 1.46, respectively (Fig. 2a). This again shows that our preparation consists of pure His-RnlA dimer lacking RnlB.

3.2. Purification and biophysical characterization of the RnlA–RnlB-His preparation

In our efforts to co-purify RnlA in complex with its antitoxin, the His tag was transferred to the C-terminus of RnlB.

The newly His-tagged rnlAB operon was cloned into a pET-21b vector for expression in E. coli BL21 (DE3) cells. The protein was purified to homogeneity by Ni–NTA affinity chromatography followed by two consecutive gel filtrations. The RnlA–RnlB-His-containing fractions that eluted from the Ni–NTA column were applied onto a Superdex 200 size-exclusion chromatography column. SDS–PAGE analysis of these fractions showed the presence of a 20 kDa contaminant that elutes together with the RnlA–RnlB-His complex. Therefore, the Superdex 200 fractions were concentrated and applied onto a Superdex 75 column for separation of this
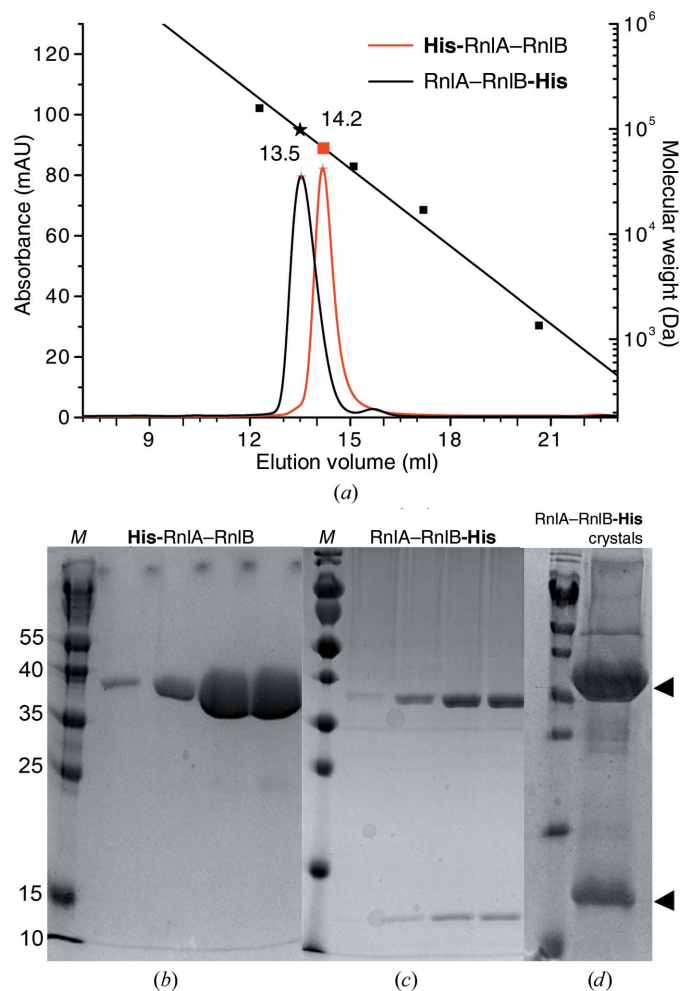
Figure 1
(a) Analytical size-exclusion chromatography profiles of His-RnlA–RnlB (red) and RnlA–RnlB-His (black) samples on a Superdex 200 Increase column. The elution volumes of the molecular-weight standards are plotted as black squares (bovine γ-globulin, 158 000 Da; chicken ovalbumin, 44 000 Da; horse myoglobin, 17 000 Da; vitamin B$_{12}$, 1350 Da). The red square and the black star represent the elution positions of the His-RnlA–RnlB and RnlA–RnlB-His peaks, respectively. (b, c, d) 15% SDS–PAGE gels of purified fractions for His-RnlA–RnlB (b), RnlA–RnlB-His (c) and the redissolved crystals of RnlA–RnlB-His (d). Arrowheads mark the positions of the RnlA and RnlB-His proteins on the gels. In (b) the only visible band corresponds to His-RnlA, and RnlB is not detected by Coomassie staining. RnlA and RnlB-His bands are both visible on the gels in (c) and (d) (the presence of RnlB-His was further confirmed by an anti-His Western blot). The Thermo Fisher Prestained Protein Ladder 10 to 180 kDa is shown as a reference in lane M.

contaminant. 1 mg pure RnlA–RnlB-His complex was finally obtained per litre of culture. This RnlA–RnlB-His preparation eluted from a Superdex Increase 200 column at a volume of 13.5 ml, corresponding to an estimated molecular weight of 97 kDa (Fig. 1a), which is a higher value than that estimated for the His-RnlA–RnlB sample measured under the same conditions, and could correspond to a 2:2 RnlA:RnlB-His complex. This time, the presence of RnlB-His was confirmed by SDS–PAGE analysis and an anti-His-tag Western blot, as shown in Fig. 1(c).

SEC–SAXS data for the RnlA–RnlB-His preparation were measured on the SWING beamline. Again, the RnlA–RnlB-His preparation, concentrated to 5.9 mg ml^{-1}, was applied onto a Shodex column coupled to a capillary for SAXS measurements. The average of the scattering curves for the

peak range shows a good dispersion up to q values of 0.4 Å^{-1} (Fig. 2c). The R_g determined via the Guinier plot for this data set has a value of 34.6 Å (Fig. 2d), which is very close to the value determined for the His-RnlA–RnlB sample. However, the shape of the scattering curves differs greatly and the fitting of the experimental curve from the RnlA–RnlB-His preparation to the theoretical SAXS curves for the RnlA biological assembly and crystallographic dimers (PDB entry 4i8o) show χ^2 values of 55.4 and 24.2, respectively (Fig. 2c). The molecular weight estimated from analysis of the Porod volume showed a median value of 99.53 ± 3.83 kDa, while analysis of the volume of correlation yielded a median value of 115.47 kDa. These values both agree well with the theoretical molecular weight of a 2:2 RnlA:RnlB-His complex, the value for which is 109.8 kDa.
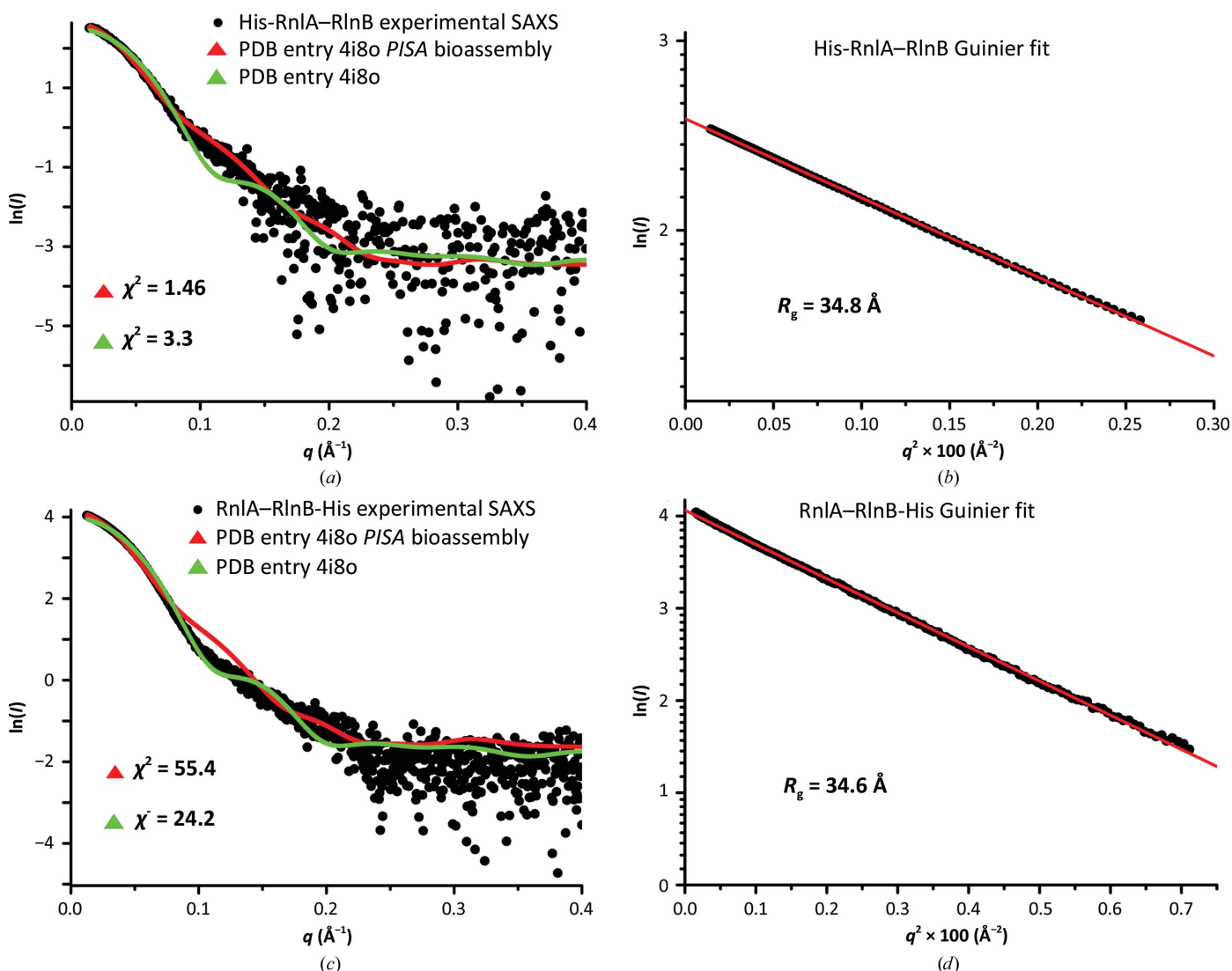
Figure 2
Small-angle X-ray scattering. (a, b) Scattering curves after background subtraction (a) and Guinier plots (b) for His-RnlA–RnlB (applied at 2.47 mg ml^{-1} onto a Shodex column). The fit to the theoretical SAXS curve for the biological RnlA dimer (red curve) rendered a χ^2 value of 1.46, while the fit to the theoretical SAXS curve for the crystallographic dimer in PDB entry 4i8o (green curve) showed a χ^2 value of 3.3. (c, d) Scattering curves after background subtraction (c) and Guinier plots (d) for RnlA–RnlB-His (applied at 5.9 mg ml^{-1} onto a Shodex column). The fit to the theoretical SAXS curves for the biological RnlA dimer (red curve) and the crystallographic dimer in PDB entry 4i8o (green curve) showed χ^2 values of 55.4 and 24.2, respectively.

Table 2
Crystallization.

The conditions listed in the table are those for the crystals that diffracted best.

Construct	His-RnlA–RnlB	RnlA–RnlB-His
Method	Sitting-drop vapour diffusion	Hanging-drop vapour diffusion
Plate type	96-well IntelliPlate (Hampton Research)	48-well VDX greased plate (Hampton Research)
Temperature (K)	293	293
Protein concentration (mg ml^{-1})	6–18	22–44
Buffer composition of protein solution	20 mM Tris–HCl pH 8, 150 mM NaCl, 1 mM tris(2-carboxyethyl)phosphine	20 mM Tris–HCl pH 8, 150 mM NaCl, 1 mM tris(2-carboxyethyl)phosphine
Composition of reservoir solution	0.1 M MES monohydrate pH 6.5, 12% PEG 20 000 (Crystal Screen 2 condition No. 22); 0.1 M Tris–HCl pH 8.5, 0.1 M potassium chloride, 3% PEG 6000 (JBScreen Classic 4 condition A3)	0.1 M bis-Tris pH 6, 15%(w/v) SOKALAN CP 5 (MIDAS condition No. 2-36); 0.1 M Tris–HCl pH 8.5, 25%(w/v) SOKALAN CP 5 (MIDAS condition No. 2-46)
Volume and ratio of drop	0.1 µl; 1:1 protein:buffer ratio	0.5 µl; 1:1 protein:buffer ratio
Volume of reservoir (µl)	100	100

In order to further assess the stoichiometry of the complex in solution, the RnlA–RnlB-His sample in ammonium acetate buffer was analysed by native mass spectrometry. The spectrum recorded for this sample at a concentration of 1.8 µM shows peaks corresponding to different charge states of complexes with 2:2 and 2:1 RnlA:RnlB-His stoichiometries (Fig. 3a). This result confirms the presence of both RnlA and RnlB in a heterotetrameric complex in solution, as first suggested by the SAXS measurements and the analytical SEC experiments performed using this sample.

3.3. X-ray crystallography

Both protein preparations were subjected to crystallization screening. Crystals grew from the His-RnlA–RnlB preparation after a week in condition No. 22 of Crystal Screen 2

(Table 2) supplemented with 0.2 µl of condition F11 [0.2%(w/v) pyridoxal hydrochloride, 0.2%(w/v) 2′-deoxyadenosine 5′-monophosphate, 0.2%(w/v) guanosine 5′-diphosphate sodium salt, 0.2%(w/v) nalidixic acid, 0.2%(w/v) uridine 5′-diphospho-N-acetylglucosamine sodium salt, 0.02 M HEPES sodium pH 6.8] from the Silver Bullets Bio crystallization additive screen (Hampton Research). Crystals were also observed in condition A3 of JBScreen Classic 4 (Table 2; Fig. 4a). The crystals obtained in these two conditions are morphologically similar and have the same unit cell and space group ($P2_12_12_1$; $a = 64.32$, $b = 100.80$, $c = 154.09$ Å). A full data set was collected from a crystal grown in the first condition that diffracted to 3.0 Å resolution (Table 3). The unit cell and space group differ from those reported previously for His-RnlA (Wei $et\ al.$, 2013) and the volume of the asymmetric unit is slightly smaller (249 755 versus 273 262 Å^3). Assuming the presence of only His-RnlA,
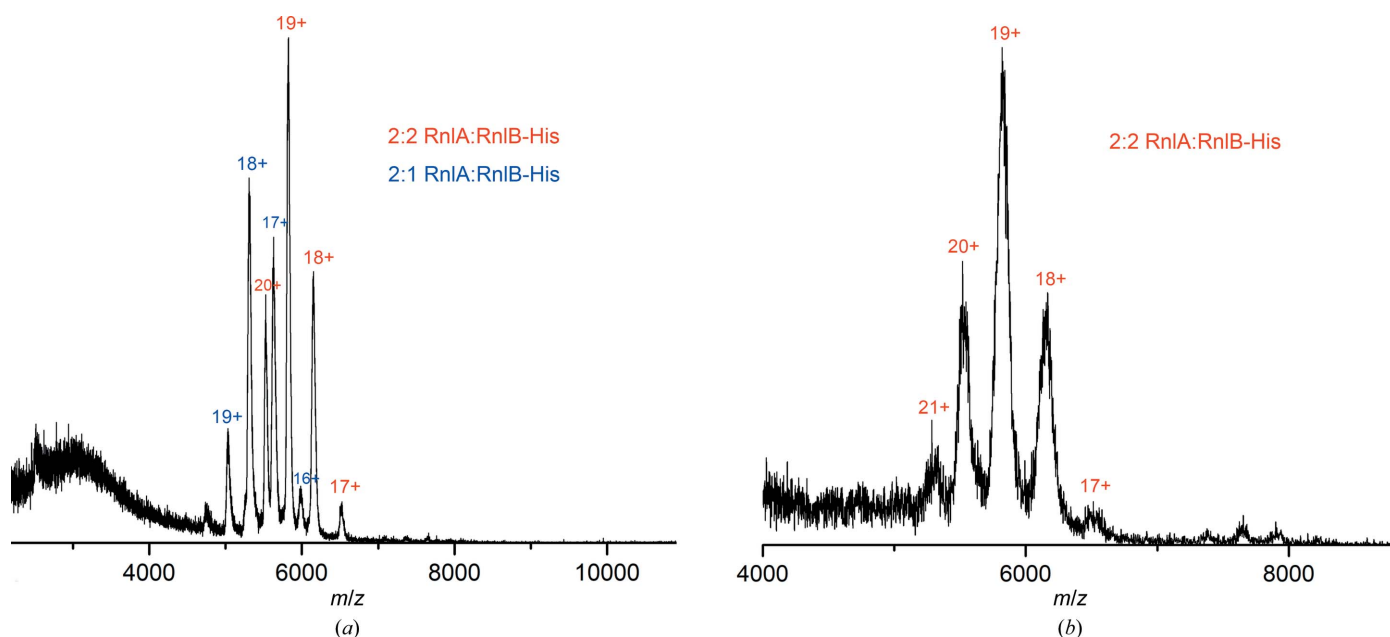
Figure 3
Native mass-spectrometric analysis of RnlA–RnlB-His samples. Native mass spectra of (a) the RnlA–RnlB-His sample before crystallization and (b) resolubilized crystals after diffraction. The measured and theoretical masses of the complexes are indicated. For both samples distributions of 2×RnlA and 2×RnlB (red charge states) were detected, whereas in the sample before crystallization (a) the complex lacking one RnlB is also present (blue charge states). Critical voltages and pressures used during the measurements were 120 V on the sampling cone, 5 V trap-collision energy for the sample in (a) and 50 V trap-collision energy for the sample in (b).

Table 3
Data collection and processing.

	His-RnlA–RnlB	RnlA–RnlB-His
Diffraction source	ID23-1, ESRF	PROXIMA-2A, SOLEIL
Wavelength (Å)	0.97	0.98
Temperature (K)	100	100
Detector	PILATUS 6M	EIGER X 9M
Crystal-to-detector distance (mm)	556.67	254.69
Rotation range per image (°)	0.1	0.1
Total rotation range (°)	360	360
Space group	$P2_12_12_1$	$C2$
a, b, c (Å)	64.32, 100.80, 154.09	243.32, 133.58, 55.64
α, β, γ (°)	90, 90, 90	90, 95.11, 90
Mosaicity (°)	0.10	0.12
Resolution range (Å)	47.9–2.98 (3.09–2.98)	48.78–2.63 (2.73–2.63)
Total No. of reflections	144889 (11998)	350162 (30565)
No. of unique reflections	20824 (1880)	51666 (4790)
Completeness (%)	99.01 (90.9)	99.09 (92.0)
Multiplicity	7.0 (6.4)	6.8 (6.4)
$\langle I/\sigma(I)\rangle$	9.36 (1.13)	12.10 (1.50)
R_{merge}	0.18 (1.73)	0.11 (0.82)
R_{meas}	0.19 (1.89)	0.12 (0.89)
$CC_{1/2}$	0.99 (0.52)	0.99 (0.79)
CC^*	0.99 (0.82)	0.99 (0.94)
Overall B factor from Wilson plot (Å^2)	80.6	70.4

Matthews analysis (Matthews, 1968) agrees with the asymmetric unit containing a His-RnlA dimer, with a V_M value of 2.96 Å^3 Da^{-1}, a solvent content of 58.44% and a probability of 0.99.

For the RnlA–RnlB-His preparation, crystals were obtained through variation of the protein concentration (20–40 mg ml^{-1}) and concentration of the hit condition in water from 20 to 80% using condition No. 2-36 of the MIDAS screen from Molecular Dimensions [0.1 M bis-Tris pH 6, 15%(w/v) SOKALAN CP 5] and condition No. 2-46 of the same screen [0.1 M Tris pH 8.5, 25%(w/v) SOKALAN CP 5]. These optimization plates were incubated at 293 K and large plate-shaped crystals were observed after seven days (Fig. 4b). These crystals belonged to space group $C2$, with unit-cell parameters $a = 243.32$, $b = 133.58$, $c = 55.64$ Å, $\beta = 95.11°$, and diffracted to 2.6 Å resolution (Table 3).

SDS–PAGE analysis as well as native mass-spectrometric analysis of washed and redissolved crystals of RnlA–RnlB-His clearly indicated the presence of both RnlA and RnlB-His in a 2:2 stoichiometry (Figs. 1d and 3b), showing that in this case it is indeed the complex that has been crystallized. Matthews analysis (Kantardjieff & Rupp, 2003) suggests the presence of both RnlA and RnlB-His in a 2:2 stoichiometry in the asymmetric unit, with a V_M of 2.23 Å^3 Da^{-1} and a corresponding solvent content of 44.86%. While SDS–PAGE and mass spectrometry show that both proteins are intact without any signs of significant degradation (Figs. 1d and 3b), we failed to obtain a molecular-replacement solution using the published structure of His-RnlA (PDB entry 4i8o; Wei *et al.*, 2013). Furthermore, attempts to solve the structure by repeating the molecular-replacement search using individual domains were also not successful, and only two copies of the C-terminal domain of His-RnlA could be placed so far in a dimeric

arrangement that does not reproduce the native dimer in PDB entry 4i8o. This partial solution (LLG = 686), however, was insufficient to obtain an interpretable map for the missing RnlA domains and the RnlB structure. This indicates that upon binding to RnlB, RnlA is likely to undergo significant conformational changes and that structure solution will require experimental phasing.

A question remains as to why the His-RnlA–RnlB and RnlA–RnlB-His preparations behave so differently. According to Wei *et al.* (2013), RnlB is extremely unstable and degrades when cells are disrupted, resulting in a preparation of pure His-RnlA. Our current results, however, indicate that replacement of the affinity tag may influence the affinity between the proteins. When it is placed at the C-terminus of
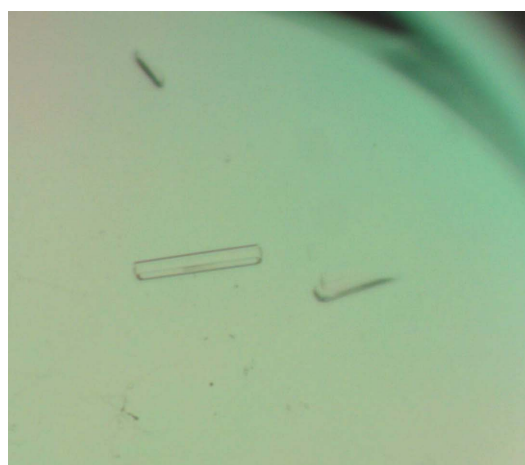
(a)
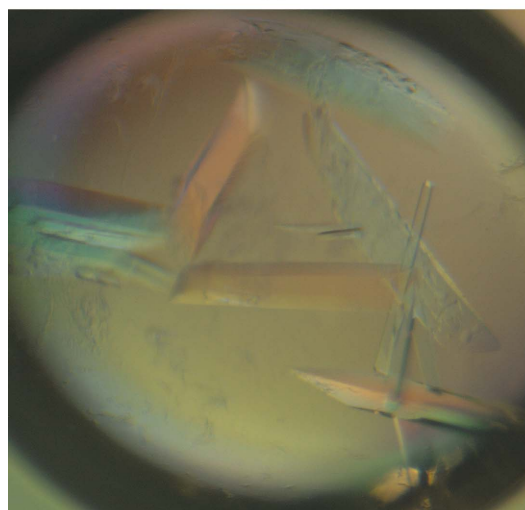
(b)

Figure 4
(a) Crystals from the His-RnlA–RnlB preparation (7 mg ml^{-1}) obtained in 0.1 M MES monohydrate pH 6.5, 12% PEG 20 000 supplemented with 0.2%(w/v) pyridoxal hydrochloride, 0.2%(w/v) 2′-deoxyadenosine 5′-monophosphate, 0.2%(w/v) guanosine 5′-diphosphate sodium salt, 0.2%(w/v) nalidixic acid, 0.2%(w/v) uridine 5′-diphospho-N-acetylglucosamine sodium salt, 0.02 M HEPES sodium pH 6.8. (b) Crystals of the RnlA–RnlB-His complex (44 mg ml^{-1}) obtained in 50% condition No. 2-46 of the MIDAS crystal screen [0.1 M Tris pH 8.5, 25%(w/v) SOKALAN CP 5].

RnlB, a stable complex can be formed that shows a stoichiometric composition and that readily crystallizes. On the other hand, a polyhistidine tag at the N-terminus of RnlA may interfere with RnlB binding, weakening the interaction between the proteins. Within the cell, possibly owing to excess production of RnlB (Otsuka *et al.*, 2010), the weaker affinity may still be sufficient to neutralize RnlA, but once diluted, the complex may dissociate when the His tag is placed at the N-terminus of RnlA.

Funding information

References

Dy, R. L., Richter, C., Salmond, G. P. C. & Fineran, P. C. (2014). *Annu. Rev. Virol.* **1**, 307–331.

Evans, P. (2006). *Acta Cryst.* D**62**, 72–82.

Franke, D., Petoukhov, M. V., Konarev, P. V., Panjkovich, A., Tuukkanen, A., Mertens, H. D. T., Kikhney, A. G., Hajizadeh, N. R., Franklin, J. M., Jeffries, C. M. & Svergun, D. I. (2017). *J. Appl. Cryst.* **50**, 1212–1225.

Gerdes, K., Christensen, S. K. & Løbner-Olesen, A. (2005). *Nat. Rev. Microbiol.* **3**, 371–382.

Gerdes, K., Rasmussen, P. B. & Molin, S. (1986). *Proc. Natl Acad. Sci. USA*, **83**, 3116–3120.

Goormaghtigh, F., Fraikin, N., Putrinš, M., Hallaert, T., Hauryliuk, V., Garcia-Pino, A., Sjödin, A., Kasvandik, S., Udekwu, K., Tenson, T., Kaldalu, N. & Van Melderen, L. (2018). *MBio*, **9**, e00640-18.

Guglielmini, J. & Van Melderen, L. (2011). *Mob. Genet. Elem.* **1**, 283–290.

Hanahan, D., Jessee, J. & Bloom, F. R. (1991). *Methods Enzymol.* **204**, 63–113.

Harms, A., Brodersen, D. E., Mitarai, N. & Gerdes, K. (2018). *Mol. Cell*, **70**, 768–784.

Hazan, R. & Engelberg-Kulka, H. (2004). *Mol. Genet. Genomics*, **272**, 227–234.

Helaine, S., Cheverton, A. M., Watson, K. G., Faure, L. M., Matthews, S. A. & Holden, D. W. (2014). *Science*, **343**, 204–208.

Kabsch, W. (2010). *Acta Cryst.* D**66**, 125–132.

Kantardjieff, K. A. & Rupp, B. (2003). *Protein Sci.* **12**, 1865–1871.

Koga, M., Otsuka, Y., Lemire, S. & Yonesaki, T. (2011). *Genetics*, **187**, 123–130.

Korch, S. B., Henderson, T. A. & Hill, T. M. (2003). *Mol. Microbiol.* **50**, 1199–1213.

Laemmli, U. K. (1970). *Nature*, **227**, 680–685.

Legrand, P. (2017). *XDSME: XDS Made Easier.* https://github.com/legrandp/xdsme.

Liebschner, D., Afonine, P. V., Baker, M. L., Bunkóczi, G., Chen, V. B., Croll, T. I., Hintze, B., Hung, L.-W., Jain, S., McCoy, A. J., Moriarty, N. W., Oeffner, R. D., Poon, B. K., Prisant, M. G., Read, R. J., Richardson, J. S., Richardson, D. C., Sammito, M. D., Sobolev, O. V., Stockwell, D. H., Terwilliger, T. C., Urzhumtsev, A. G., Videau, L. L., Williams, C. J. & Adams, P. D. (2019). *Acta Cryst.* D**75**, 861–877.

Loris, R. & Garcia-Pino, A. (2014). *Chem. Rev.* **114**, 6933–6947.

Matthews, B. W. (1968). *J. Mol. Biol.* **33**, 491–497.

Moyed, H. S. & Bertrand, K. P. (1983). *J. Bacteriol.* **155**, 768–775.

Nonaka, G., Blankschien, M., Herman, C., Gross, C. A. & Rhodius, V. A. (2006). *Genes Dev.* **20**, 1776–1789.

Otsuka, Y. (2016). *Curr. Genet.* **62**, 379–382.

Otsuka, Y., Koga, M., Iwamoto, A. & Yonesaki, T. (2007). *Genes Genet. Syst.* **82**, 291–299.

Otsuka, Y., Miki, K., Koga, M., Katayama, N., Morimoto, W., Takahashi, Y. & Yonesaki, T. (2010). *Genetics*, **185**, 823–830.

Otsuka, Y. & Yonesaki, T. (2005). *Genetics*, **169**, 13–20.

Otsuka, Y. & Yonesaki, T. (2012). *Mol. Microbiol.* **83**, 669–681.

Page, R. & Peti, W. (2016). *Nat. Chem. Biol.* **12**, 208–214.

Ramisetty, B. C., Ghosh, D., Roy Chowdhury, M. & Santhosh, R. S. (2016). *Front. Microbiol.* **7**, 1882.

Studier, F. W., Rosenberg, A. H., Dunn, J. J. & Dubendorff, J. W. (1990). *Methods Enzymol.* **185**, 60–89.

Sun, C., Guo, Y., Tang, K., Wen, Z., Li, B., Zeng, Z. & Wang, X. (2017). *Front. Microbiol.* **8**, 840.

Towbin, H., Staehelin, T. & Gordon, J. (1979). *Proc. Natl Acad. Sci. USA*, **76**, 4350–4354.

Unterholzner, S. J., Poppenberger, B. & Rozhon, W. (2013). *Mob. Genet. Elem.* **3**, e26219.

Van Melderen, L. (2010). *Curr. Opin. Microbiol.* **13**, 781–785.

Van Melderen, L. & Saavedra De Bast, M. (2009). *PLoS Genet.* **5**, e1000437.

Wan, H., Otsuka, Y., Gao, Z.-Q., Wei, Y., Chen, Z., Masuda, M., Yonesaki, T., Zhang, H. & Dong, Y.-H. (2016). *Mol. Microbiol.* **101**, 757–769.

Wei, Y., Gao, Z., Zhang, H. & Dong, Y. (2016). *Biochem. Biophys. Res. Commun.* **472**, 592–597.

Wei, Y., Gao, Z.-Q., Otsuka, Y., Naka, K., Yonesaki, T., Zhang, H. & Dong, Y.-H. (2013). *Mol. Microbiol.* **90**, 956–965.

Whitaker, J. R. (1963). *Anal. Chem.* **35**, 1950–1953.

Yamaguchi, Y. & Inouye, M. (2011). *Nat. Rev. Microbiol.* **9**, 779–790.